Kohlmeyer et al.
Clinical Cancer Research
Supplemental Figures and Tables

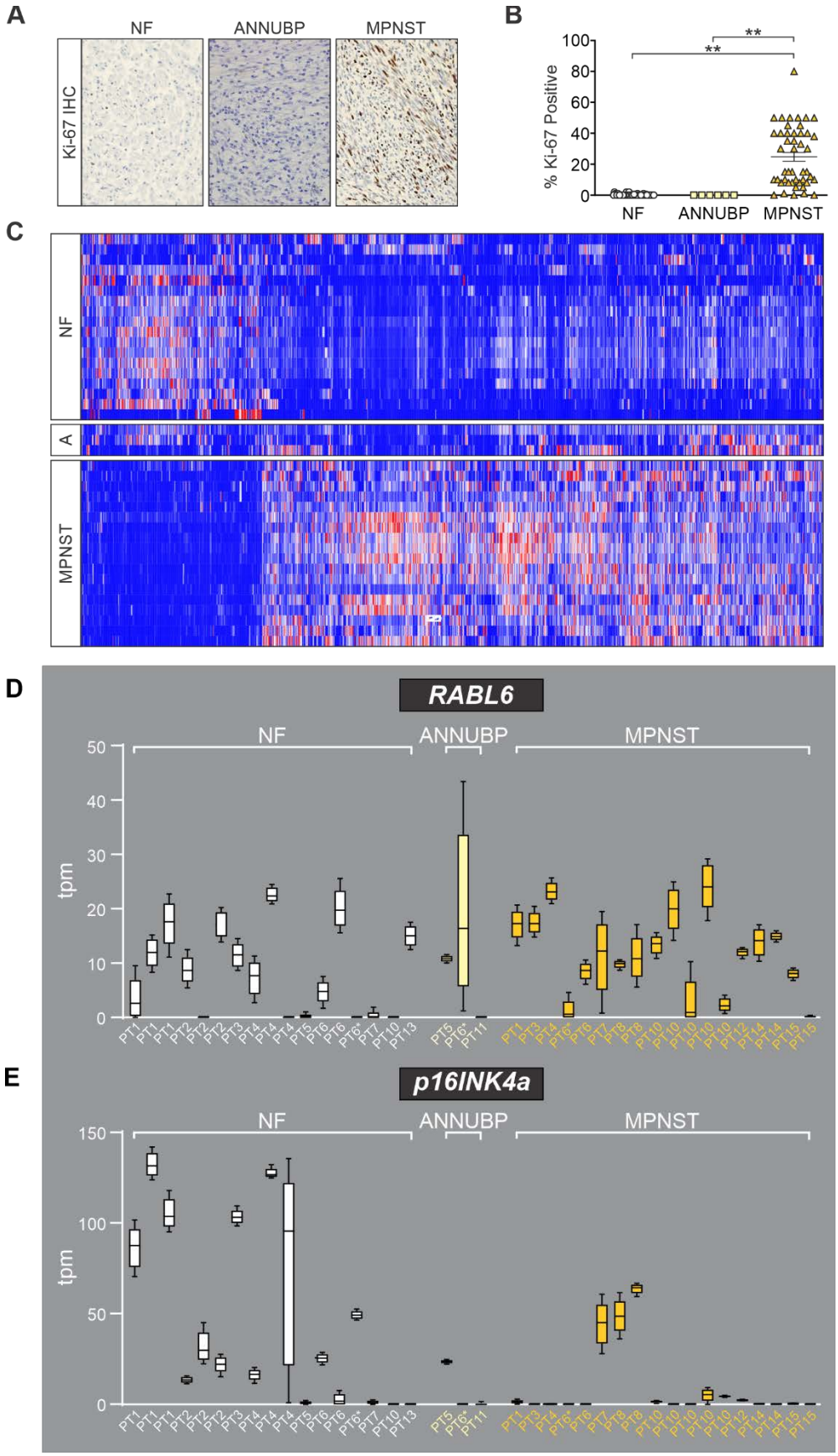
A
NF
ANNUBP
MPNST
Ki-67 IHC
B
% Ki-67 Positive
100
80
60
40
20
0
**
**
NF
ANNUBP
MPNST
C
NF
A
MPNST
D
RABL6
NF
ANNUBP
MPNST
tpm
50
40
30
20
10
0
E
p16INK4a
NF
ANNUBP
MPNST
tpm
150
100
50
0

Supplemental Figure 1. Molecular alterations during the PNF to MPNST transition in NF1 patient specimens. **(A)** IHC staining of Ki-67 in TMAs of patient-matched NF (mainly plexiform NFs), ANNUBPs, and MPNSTs. Images at 400X magnification. **(B)** Percent positivity of Ki-67 staining in NF, ANNUBP, and MPNST samples. C: Error bars, SEM. P-value, Student's *t*-test, **p<0.01. **(C)** Heat-map of RNA-Seq data with hierarchical clustering of differentially expressed genes (q value < 0.20 and log2 fold change >1.5 or <-1.5) between paired patient NF/PNFs, ANNUBPs, and MPNSTs. Genes were categorized by IPA software. Red, relatively increased expression; blue, relatively decreased expression. Genes can be found in Supplemental Table 2. The relative abundance of *RABL6* **(D)** and *p16INK4a* **(E)** transcripts in the indicated patient (PT) samples were determined from RNA-Seq data and presented as transcripts per million (tpm, normalized expression units). *, PT6 had one lesion displaying all three stages of transformation; NF, plexiform neurofibroma; ANNUBP, atypical neurofibromatosis neoplasm of unidentified biologic potential; MPNST, malignant peripheral nerve sheath tumor. Many patients had multiple benign NF and/or transformed MPNST tumors. Note that not all patient samples yielded RNA of sufficient quality or quantity for RNA-Seq analysis; consequently, not all specimens examined by IHC are included in the datasets in (D) and (E).

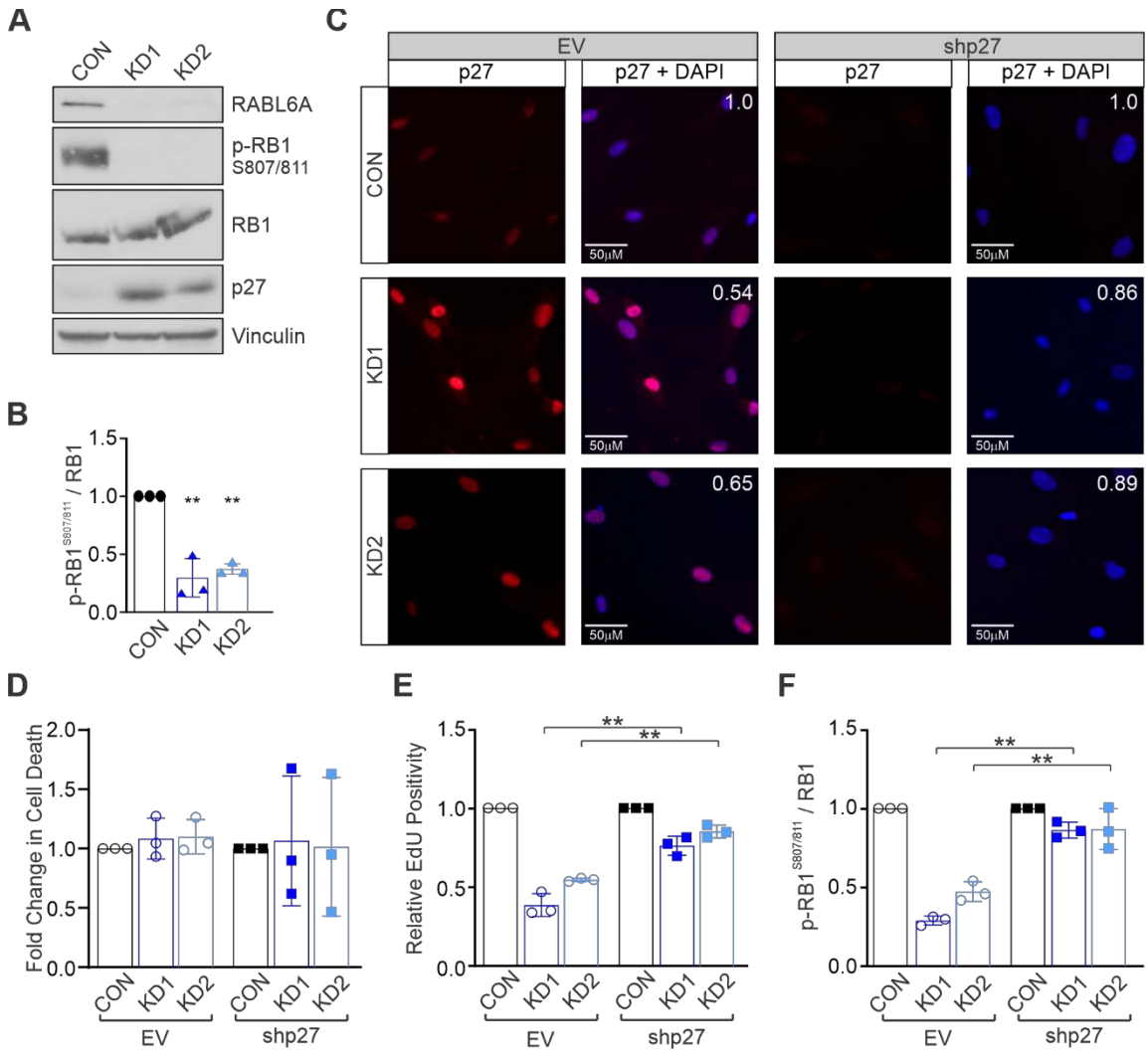

Supplemental Figure 2. RABL6A promotes NHSC growth via the RB1-p27 pathway. NHSCs were transduced with control (CON) or *RABL6A* shRNA viruses (KD1 and KD2). In C-F, cells were first infected with empty vector (EV) or *p27* shRNA viruses before CON, KD1 or KD2 virus infection. **(A)** Representative westerns show loss of RABL6A causes upregulation of p27 protein and decreased phosphorylation of RB1 at S807/811. **(B)** Quantification of p-RB1 S807/811 immunofluorescence (IF) recapitulates the decrease in phosphorylated RB1 observed in (A) following RABL6A depletion. **(C)** Representative IF images show loss of p27 as expected in *shp27* expressing cells compared to EV. These images also demonstrate loss of RABL6A in EV cells causes the expected upregulation of p27. DAPI, blue; p27, red; overlay, purple. Top right corner, cell ratio relative to control cells. **(D)** Quantification of the fold change in cell death reveals no difference in EV versus *shp27* cells showing loss of RABL6A does not induce NHSC death. **(E)** Quantification of EdU positivity shows p27 inactivation rescues DNA synthesis in RABL6A depleted NHSCs. **(F)** Quantification of p-RB1 S807/811 IF shows restoration of RB1 phosphorylation in NHSCs co-depleted of p27 and RABL6A. Data in B, D, E and F are from three or more independent experiments. Error bars, SD from mean. P-value, Student's *t*-test. **, p<0.01.

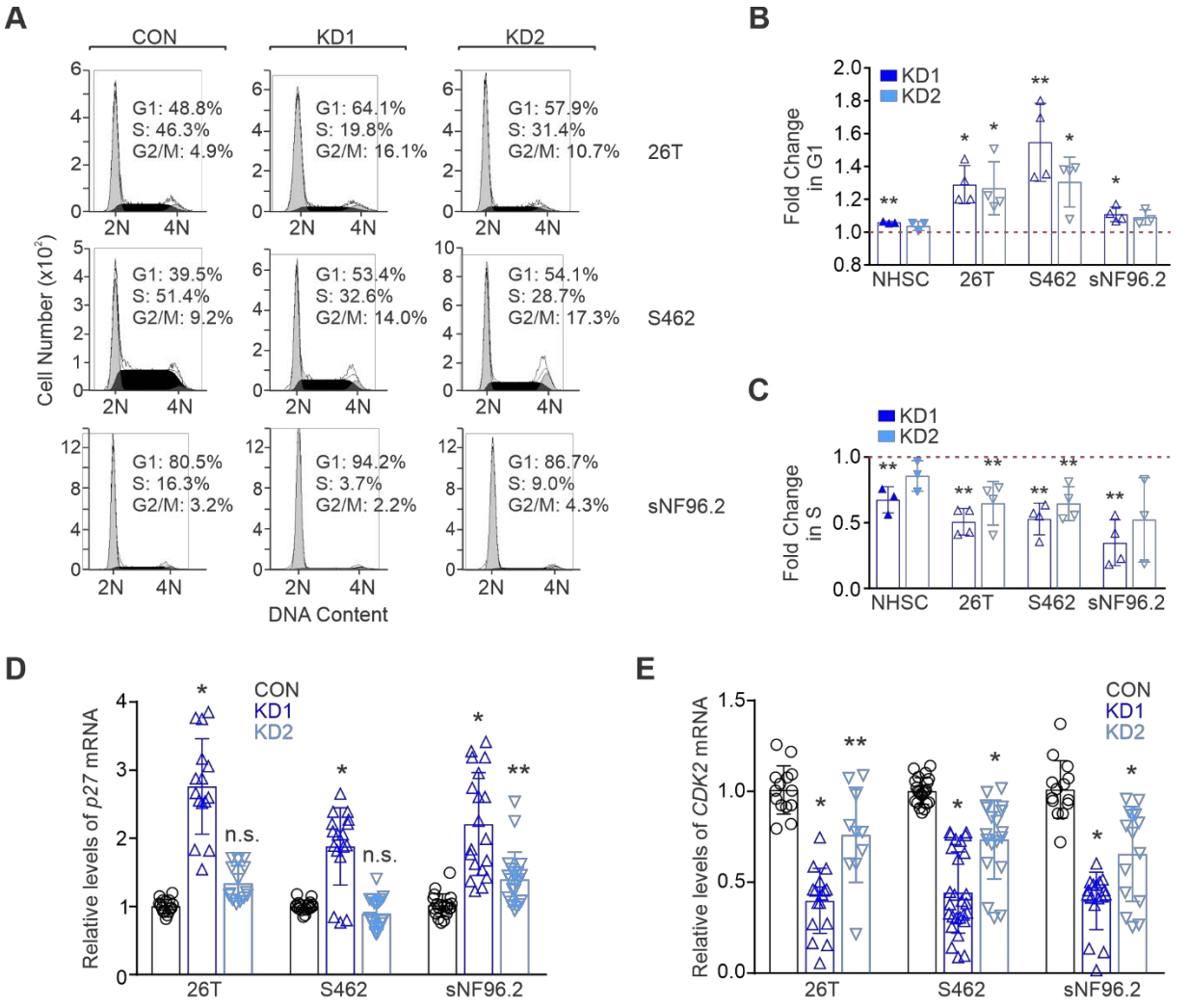

Supplemental Figure 3. RABL6A is required for MPNST cell cycling from G1 to S phase, affecting associated molecular players. (A) Representative histograms of DNA content analyses in MPNST cell lines show RABL6A loss causes G1 accumulation and decreased S phase. **(B)** Quantification of the fold change in G1 phase after RABL6A KD in NHSCs and MPNST cell lines shows loss of RABL6A causes an accumulation in G1 phase versus CON cells (set at 1.0, dashed red line). **(C)** Quantification of the fold change in S phase after RABL6A KD shows loss of RABL6A significantly reduces the percentage of cells in S phase versus CON (set at 1.0, dashed red line). Quantitative RT-PCR analyses were performed in the indicated MPNST cell lines following expression of control (CON) or RABL6A shRNAs (KD1 and KD2). Results (from 3 or more independent experiments) were normalized to *GAPDH* mRNA levels. **(D)** Moderate to no upregulation of *p27* mRNA is caused by RABL6A knockdown. **(E)** Significant downregulation of *CDK2* mRNA results from RABL6A depletion (more so in KD1 cells). Data in A-E are from three of more independent experiments, with triplicate samples assayed in D and E. Panels B-E: Error bars, SD from mean. P-value, Student's *t*-test with Dunnett's correction for KD versus CON; *, p<0.05; **, p<0.01.

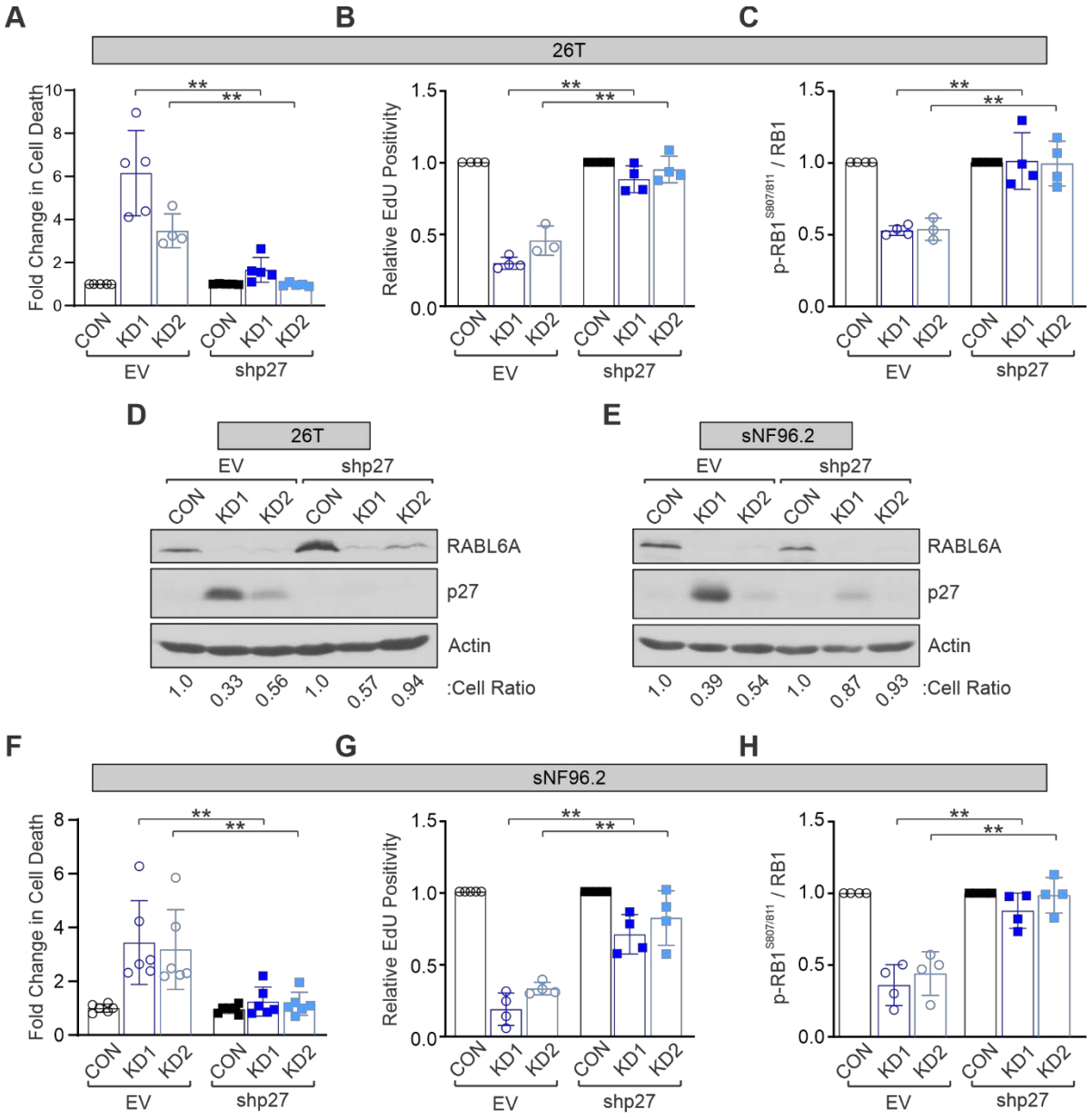

Supplemental Figure 4. RABL6A promotes MPNST cell proliferation and survival via p27-RB1 inactivation. 26T (panels A-D) and sNF96.2 (panels E-H) MPNST cells were transduced with empty vector (EV) or *p27* shRNA viruses and subsequently infected with control (CON) or RABL6A shRNA viruses (KD1 and KD2). **(A, F)** Quantification of the fold change in cell death after RABL6A knockdown shows that p27 inactivation rescues cell death caused by RABL6A loss. **(B, G)** Quantification of EdU positivity shows p27 inactivation rescues DNA synthesis in RABL6A depleted cells. **(C, H)** Quantification of nuclear phospho-RB1 S807/811 by immunofluorescence shows loss of p27 partially restores p-RB1 in RABL6A depleted cells. **(D, E)** Representative westerns verify *RABL6A* knockdown with or without p27 co-depletion in cells expressing *p27* shRNA. Below, cell ratio (relative to control cells) for the displayed experiment. Data in A-C and F-H are from three or more independent experiments. Error bars, SD from mean. P-value, Student's *t*-test. **, p<0.01.

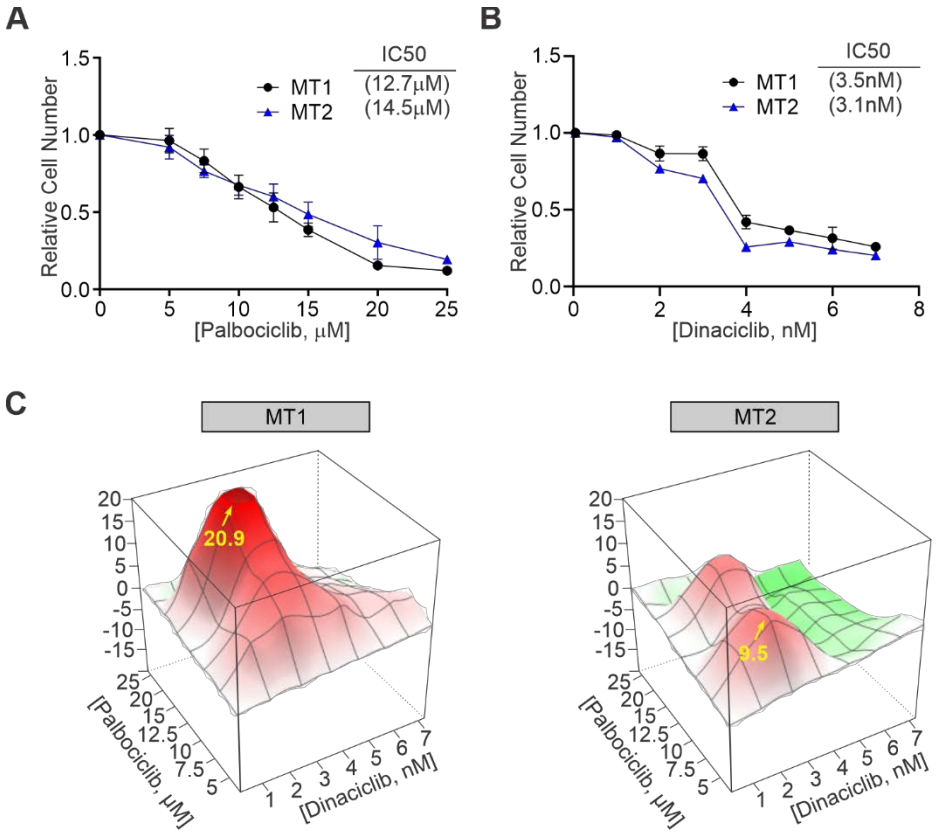

Supplemental Figure 5. Patient derived MPNST cultures are inhibited by palbociclib, dinaciclib and the combination. MT1 and MT2 cultures were generated from two separate metastatic MPNSTs within one NF patient. Cells were treated for three days with the indicated drug concentrations of (A) palbociclib, (B) dinaciclib, or (C) both compounds. **(A)** Graph of relative cell number, which was assessed by AlamarBlue following treatment with palbociclib. IC50 values indicated at top right. **(B)** Graph of relative cell number in response to dinaciclib treatment, as assessed by AlamarBlue. IC50 values indicated at top right. **(C)** Contour plot showing that low dose combinations of palbociclib plus dinaciclib act synergistically against MT1 (left) and MT2 (right) cultures. Results from *in vitro* combination analysis and AlamarBlue proliferation / viability assay using the Loewe-additivity and Bliss-independence methods. Red, synergy; green, antagonism. Highest synergy value indicated in yellow.

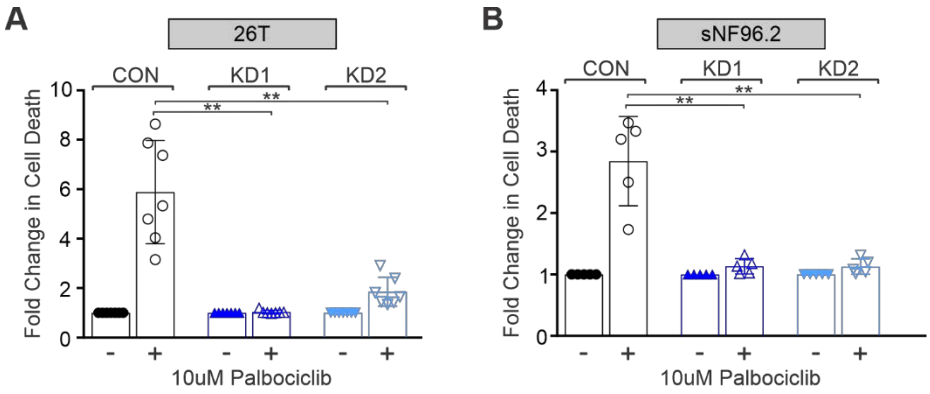

Supplemental Figure 6. MPNST cell lines, 26T and sNF96.2, are killed in vitro by the CDK4/6 inhibitor, palbociclib, in a RABL6A-dependent manner. Fold change in cell death of control (CON) versus RABL6A knockdown (KD1 and KD2) in **(A)** 26T or **(B)** sNF96.2 cells treated with vehicle (-) or 10 μM palbociclib (+). Cells lacking RABL6A show reduced cell death compared to CON cells. P-value, Student's *t*-test with Bonferroni's correction; **, p<0.01.

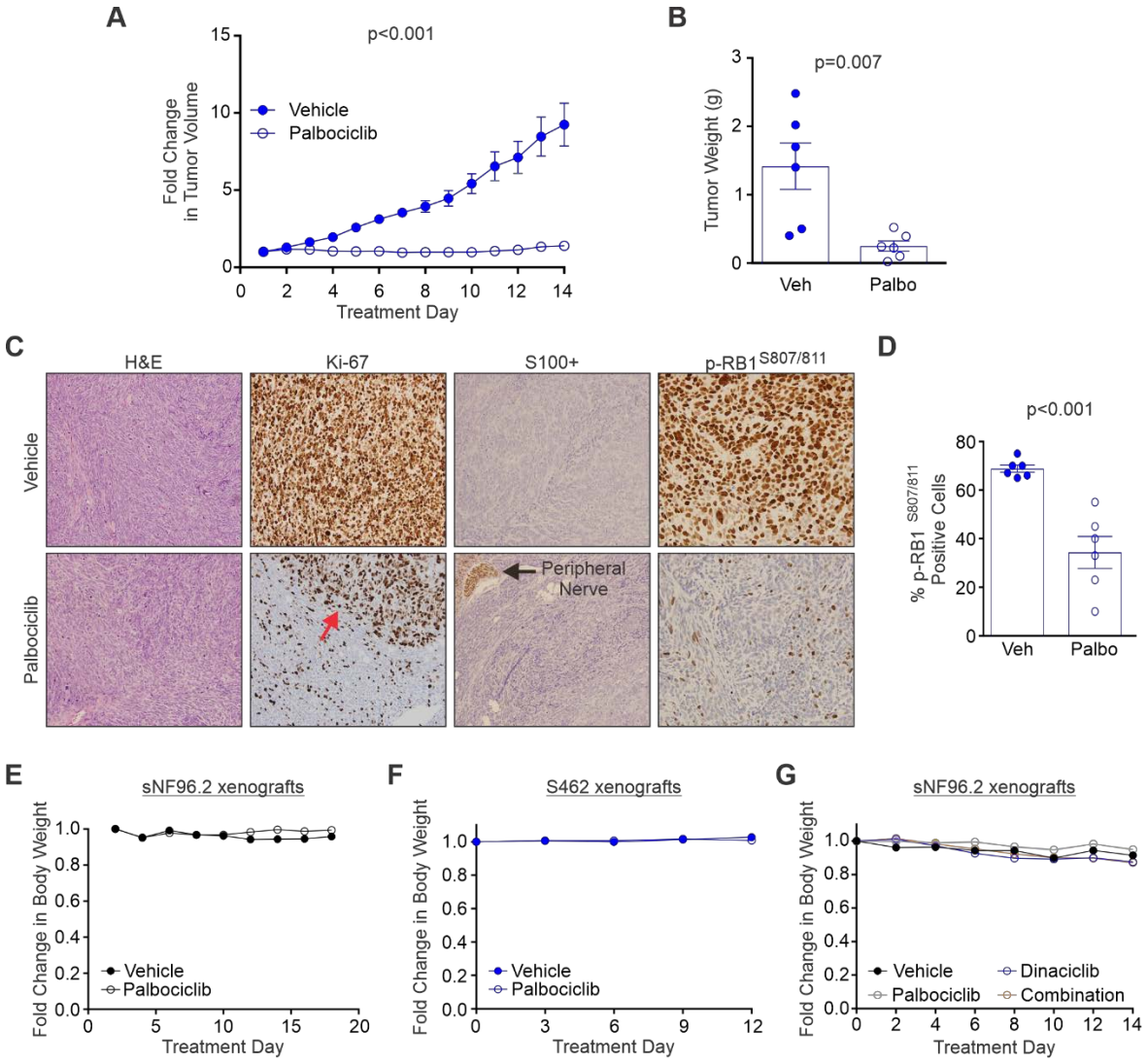

Supplemental Figure 7. **CDK4/6 inhibition significantly reduces MPNST growth *in vivo* without causing toxic side effects.** Orthotopic xenograft MPNSTs of S462 cells were generated in NSG mice. **(A)** Fold change in tumor volume in vehicle versus palbociclib treated mice. Palbociclib (25 mg/kg) or vehicle (water) was administered by oral gavage daily once tumors were approximately 200 mm^3 in size. **(B)** Comparison of tumor weights after excision show palbociclib (Palbo) significantly reduces tumor weight compared to vehicle (Veh). **(C)** H&E images and IHC staining for Ki-67, S100+, and phospho-RB1 S807/811 in tumor samples from vehicle and palbociclib treated mice. Red arrow, intra-tumoral region of high Ki-67. Black arrow, positive control of S100 staining in peripheral nerve. H&E images at 400X magnification, and IHC images at 200X magnification. **(D)** Quantification of the percent cells that stained positive by IHC for phosphorylated RB1-S807/811 in tumors from Veh or Palbo treated mice. Mouse body weights from orthotopic xenografts of **(E)** sNF96.2 cells or **(F)** S462 cells were measured at the indicated times just before and during treatment with vehicle control or palbociclib. **(G)** Mouse body weights from orthotopic xenografts of sNF96.2 cells were measured at the indicated times just before and during treatment with vehicle control, palbociclib alone, dinaciclib alone, or a combination of palbociclib and dinaciclib. Data represent the means from each treatment group. Error bars, SEM. The number of animals for each group in **(E)** is n=5; **(F)** is n=6; **(G)** is n=5 for vehicle and palbociclib treatment, and n=4 for Dinaciclib and combination treatment. A, B, D: Error bars, SEM. A: P-value determined by a generalized linear model to assess the difference between curves. B, D: P-value, Student's *t*-test.

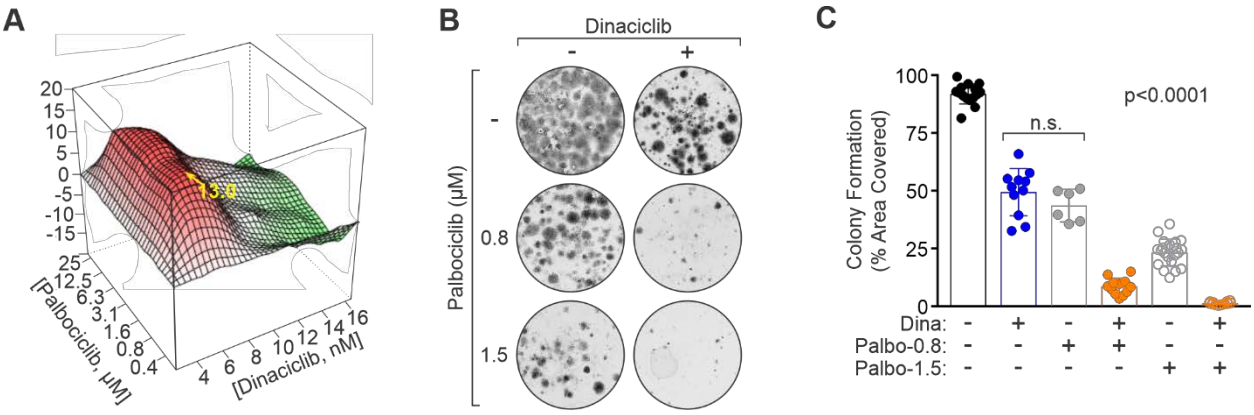

Supplemental Figure 8. **Combination therapy with multiple CDK inhibitors enhances MPNST suppression.** S462 MPNST cells were treated with dinaciclib, palbociclib or both with the indicated drug concentrations for either three days (A) or two weeks (B-C). **(A)** Contour plot showing low dose combinations of palbociclib plus dinaciclib act synergistically against S462 cells. Results from *in vitro* combination analysis and AlamarBlue proliferation / viability assay using the Loewe-additivity and Bliss-independence methods. Red, synergy; green, antagonism. Highest synergist point indicated in yellow. **(B)** Images from S462 colony formation assay after drug treatment for two weeks. **(C)** Quantification of the percentage area covered by cells from colony formation assay shows combined treatment significantly reduced clonogenic survival compared to single agent alone. P<0.0001 for all comparisons except Dina alone versus Palbo-0.8, which was not significant (n.s.); Student's t-test with Bonferroni correction.